Influence of Ion Mass on Laser-Energy Absorption and Synchrotron Radiation at Ultrahigh Laser Intensities

R. Capdessus,* E. d'Humières, and V. T. Tikhonchuk
University Bordeaux-CNRS-CEA, CELIA, UMR 5107, F-33400 Talence, France
(Received 20 February 2013; published 21 May 2013)

The role of ions in the energy absorption of a short and ultraintense laser pulse and in the synchrotron radiation generated by accelerated electrons is revisited. For laser intensities above 10^{22} W/cm^2 and plasma densities more than 10 times the critical density, the ion-to-electron mass ratio strongly affects the energy repartition between the electrons, ions, and radiation. This phenomenon is studied with a one-dimensional relativistic particle-in-cell code, taking into account the radiation reaction force. The choice of the ion mass strongly affects the energy and angular distribution of the photon emission and the electron energy distribution. This effect may be important for laboratory modeling of radiation dominated relativistic astrophysical events. It can be verified in experiments with solid hydrogen targets.

DOI: 10.1103/PhysRevLett.110.215003 PACS numbers: 52.38.−r, 41.60.−m, 52.65.Rr

The growing interest in the physics of high intensity electromagnetic fields and relativistic plasmas is motivated by the progress in design and construction of ultrahigh power laser systems that might reach the intensity of the order of 10^{24} W/cm^2 [1]. This will provide access to new physical processes such as the radiation reaction, relativistic electron dynamics, electron-positron pair production, generation of relativistic ions, etc. [2]. The electron synchrotron radiation at the laser intensities above 10^{22} W/cm^2 gives rise to the radiation reaction force [3] that strongly affects the photon emission spectrum [4] and the overall plasma dynamics [5,6]. The effect of radiation losses depends strongly on the target density, thickness, and the laser polarization. Laboratory experiments could play a fundamental role in corroborating theoretical and numerical studies of the radiation reaction on plasma dynamics [7].

It is often suggested that the interaction of a short laser pulse with overdense plasmas is dominated by the electron dynamics and the ions are playing a secondary role. Although this may be true for low laser intensities, the situation becomes more complicated in the case of ultrarelativistic laser pulses for which the quiver electron energy could be comparable with the ion rest mass. In this Letter, we demonstrate for the first time a strong influence of the ion mass on the laser-energy absorption and on the emitted synchrotron radiation in the interaction of an intense laser pulse with an overdense plasma layer. We use in this study a one-dimensional relativistic particle-in-cell code PICLS [8] that has been upgraded by taking into account the radiation reaction force and the synchrotron radiation [6].

The radiation reaction effects are described using the model developed by Sokolov [9]. The Lorentz-Abraham-Dirac equation is renormalized in order to avoid nonphysical solutions, by using a quantum electrodynamics perturbative approach. It is assumed that the characteristic electron acceleration time $t_{\mathrm{acc}} = 1/\gamma_e \omega_L$ is much larger than the radiation time $\tau_r = 2e^2/3m_e c^3 \simeq 6.2 \times 10^{-24}$ s. Here, e and m_e are the electron charge and mass, c is the light velocity, ω_L is the laser frequency, and γ_e is the electron relativistic factor. The model conserves the four-vector of the energy momentum of the electron. At the second order in τ_r/t_{acc}, the equations of electron motion are given by

$$d\mathbf{p}_e/dt = \mathbf{F}_{Le} - e\delta\beta_e \times \mathbf{B} - \gamma_e^2(\mathbf{F}_{Le} \cdot \delta\beta_e)\beta_e, \quad (1)$$

$$d\mathbf{x}_e/cdt = \beta_e + \delta\beta_e, \quad (2)$$

where

$$\delta\beta_e = \frac{(\tau_r/c)\gamma_e \mathbf{w}_e}{1 - (e\tau_r/m_e c)(\beta_e \cdot \mathbf{E})} \quad (3)$$

is the radiation correction to the electron velocity, $\mathbf{w_e}$ is the electron acceleration, and $\mathbf{F}_{Le} = -e(\mathbf{E} + \beta_e \times \mathbf{B})$ is the Lorentz force. This model is close to the Landau-Lifshitz equation [10] if the dominant term in the radiation force (1) proportional to $\gamma_e^2 \gg 1$ is retained. The main difference is in the electron trajectory equation (2), where the particle position is affected by the recoil momemtum of photons created during the time of acceleration (3). Equation (1) describes the electron dynamics, whereas Eq. (2) is related to a kinematic phenomenon. It shows that the electron velocity is not $c\beta_e$ but $c(\beta_e + \delta\beta_e)$ because this is the parameter which could be experimentally measured. Moreover, Sokolov's model (1) and (2) presents an advantage in the implementation of particle-in-cell codes by its compactness compared to the Landau-Lifshitz equation.

In the domain where the quantum electrodynamical effects are weak, the additional term in Eq. (2) has a small influence on the electron trajectory in the laser field. However, it might play a more important role in astrophysical applications, where the magnetic fields could be very strong.

For each electron accelerated in strong electromagnetic fields, the spectral intensity of the radiated field writes

$$\frac{d^2 I_r}{d\omega d\mathbf{\Omega}} = \gamma_e^3 \tau_r (\mathbf{F}_{Le} \cdot \mathbf{w}_e) \delta\left(\mathbf{\Omega} - \frac{\mathbf{p}_e}{p_e}\right) S\left(\frac{\omega}{\omega_{\rm cr}}\right), \quad (4)$$

where $S(r) = 3^{5/2}(8\pi)^{-1} r \int_r^\infty K_{5/3}(r')dr'$ describes the normalized spectral shape and K is a modified second-order Bessel function. The radiation is emitted in a narrow cone with the angle $\sim 1/\gamma_e \ll 1$ with respect to the electron propagation direction. It is modeled by a Dirac δ function in Eq. (4). In our simulations, the radiation is computed from the macroparticle trajectories, assuming the emission to be incoherent. That requires the emitted photon wavelength to be much shorter than the characteristic distance between the plasma electrons $n_e^{-1/3}$, depending on the electron density n_e. This condition imposes a limitation on the critical frequency $\omega_{\rm cr} = (3/2)\gamma_e^3 \omega_r$ of the continuous radiation:

$$\omega_{\rm cr} \gg c n_e^{1/3}. \quad (5)$$

Here, $\omega_r = |\mathbf{p}_e \times \mathbf{F}_{Le}|/p_e^2$ is the instantaneous electron rotation frequency. The total photon spectrum is calculated via postprocessing of the electron trajectories in order to save computation time. Only electrons with energies $\gamma_e \geq 10$ have been considered in the photon spectrum calculation in order to separate the radiation from the coherent electromagnetic fields described by Maxwell's equations and to satisfy the condition (5). This limitation has no effect on the electron self-force calculations, as the recoil effect of photons at these low electron energies is completely negligible.

The simulations presented in this Letter are performed in the classical regime where the electron invariant quantum parameter

$$\chi_e = \frac{e\hbar\gamma_e}{m_e^2 c^3} \sqrt{(\mathbf{E} + \beta \times \mathbf{B})^2 - (\beta \cdot \mathbf{E})^2} \quad (6)$$

is small, $\chi_e \ll 1$. In the case of a plane laser wave, $\chi_e = \gamma_e(1 - \beta_{e\|}) a_L \hbar\omega_L / m_e c^2$ depends on the dimensionless laser amplitude $a_L = eE_L/m_e\omega_L c$ and on the projection of the electron velocity on the laser wave vector direction $\beta_{e\|}$. It is necessary to account for the quantum effects for $a_L \geq 400$ when the parameter χ_e becomes larger than 1. In the first approximation, they may be described in the classical approach by multiplying the characteristic radiation time τ_r by the form factor $q(\chi_e) \simeq (1 + \chi_e)^{-4/3}$ [11].

In order to demonstrate the influence of the ion mass on the radiation effects in laser plasma interaction, we consider a circularly polarized laser pulse with the dimensionless vector potential

$$a_L(t, x) = a_0(t) \mathrm{Re}(\mathbf{y} - i\mathbf{z}) e^{-i\omega_L(t - x/c)}$$

normally incident on a plasma layer of the thickness $l = 100\lambda_L$ surrounded by $100\lambda_L$ long vacuum regions from both sides of the simulations box. The time is measured in laser periods $T_L = 2\pi/\omega_L$ and lengths in laser wavelengths $\lambda_L = T_L c$. Two temporal laser profiles are considered: a Gaussian profile with a full width at half maximum equal to $9.2T_L$ and a trapezoidal profile with linear intensity ramps over one laser period and a $16T_L$ long plateau. The maximal amplitudes were chosen in such a way that the total laser-energy fluence $\mathcal{E}_L = \int_0^{t_{\rm end}} a_0^2 dt/T_L$ is the same. The electron density was varied from 10^{-3} to $50n_c$, where $n_c = m_e\omega_L^2/4\pi e^2$ is the critical density and the laser amplitude a_0—in the range from 60 to 600. Each plasma cell had the size of $\lambda_L/80$ containing 60 macroparticles, electrons, and ions. The laser pulse interacts with the target at $t = 0$. The total simulation time $t_{\rm end} = 100T_L$.

In the simulations presented below, three ions species were considered: protons, deuterons, and infinitely massive ions; the electron density is equal to $10n_c$, and laser pulse amplitudes are $a_0 = 200$ (Gaussian) and $a_0 = 180$ (trapeziodal), corresponding to the energy fluence 5×10^9 J/cm^2 at the wavelength of 1 μm. The exception are Figs. 5 and 6, where a summary of simulations with other parameters is presented.

The energetics of laser plasma interaction is defined by the parameters $\eta_k = \mathcal{E}_k/\mathcal{E}_L$, where k stands for photons (γ), electrons (e), and ions (i): that is, $\mathcal{E}_\gamma(t)$ is the energy fluence of the photons radiated up to the time t, $\mathcal{E}_e(t)$ is the electron areal energy, and $\mathcal{E}_i(t)$ is the ion areal energy at the time t. In a similar way, $\zeta_k = d\eta_k/dt/T_L$ defines the instantaneous relative radiation intensity and the energy absorption rate by the electrons and ions.

The radiated energy and the radiated power presented in Fig. 1 demonstrate a clear difference between the plasmas made of protons and deuterons. The radiated energy decreases from more than 80% for the case of immobile ions to $\eta_\gamma \simeq 50\%$ for the case of deuterons and to less than 30% for the case of protons. This difference appears very early in the interaction, after 3–4 laser periods, and achieves the maximum at the time of 20–30. This is an unexpected

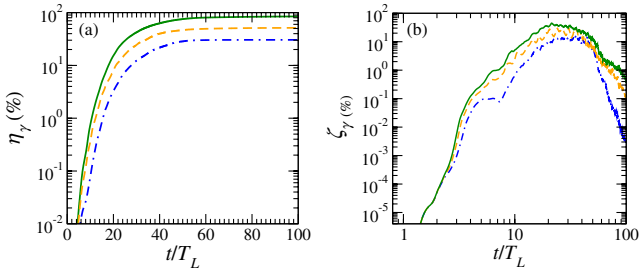

FIG. 1 (color online). Time dependence of (a) the radiated energy fluence and (b) the radiated power for the case of a Gaussian temporal profile: dash-dotted blue lines represent proton plasma, dashed orange lines represent a deuteron plasma, and solid green lines represent a plasma of immobile ions. The laser and plasma parameters are given in the text.

effect; other authors reported no evident dependence of the laser-energy absorption on the ion mass [12].

The observed effect can be explained as follows. At the beginning of the interaction, the electrons are accelerated. The ion response time depends on the ion mass. It can be estimated as $T_i = 2\pi/\omega_{pi} = (n_c m_i/m_e n_e)^{1/2} T_L$. In the case of a plasma density of $10n_c$ and $a_0 = 200$, the response time of protons and deuterons does not exceed 15–20 laser periods, as it can been seen in Fig. 1(b). Two effects contribute to this fast ion reaction. First, in such intense laser fields, the effective electron mass $\sim a_0 m_e$ is already comparable with the ion mass. Second, the radiated energy is comparable with the electron kinetic energy, and, as it has been shown in [6], the ion dynamics could be implicitly affected by the radiation reaction via the self-consistent fields. The influence of ion mass on the radiation is thus a collective effect. It increases with the plasma density. The amplitude of the charge separation electric field is comparable to the maximum amplitude of the laser field, and it increases with the ion mass. Indeed, the electrons are displaced under the action of the laser radiation pressure, and the electrostatic field increases until the ions start moving. The charge separation field amplitude thus determines the electron and the ion dynamics. The criterion that the ion motion becomes important for the radiation process may be formulated as

$$T_i \leq t_{\max}, \tag{7}$$

where $t_{\max}$ is the time of the maximum of radiation emission. The necessary condition (7) is clearly related to the collective effects occurring in the plasma due the strong dependence of $t_{\max}$ on the ion-to-electron mass ratio: $t_{\max} \simeq 40T_L$ for protons, and $t_{\max} \simeq 22T_L$ for immobile ions. The charge separation field can be assimilated to the elastic spring attached to a large mass. It needs to be stretched before forcing the mass to move. This is what happens at the plasma boundary when the laser pulse arrives. Figure 2 shows the longitudinal field at the time $t = t_{\max}$ when the radiated power is maximal. The larger the ion mass is, and the shorter time it takes to generate the charge separation field, the stronger this electric field is. In the case of immobile ions, the charge separation field attains its maximum value $E_x/E_C \simeq a_0$. The lighter the ions are, already moving at the time shown in Fig. 2, the smaller the electrostatic field is. The electrons that are accelerated in this electrostatic field toward the laser are the source of the most intense radiation. Therefore, as the ion mass is reduced, the electron kinetic energy goes down, thus reducing the radiation efficiency. Moreover, as the light ions are moving in the laser propagation direction, the electrons are dragged with them. Thus, fewer electrons can escape toward the laser, reducing the radiation even more.

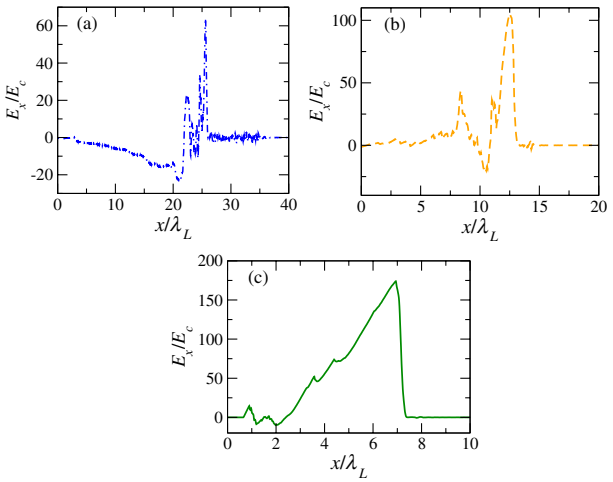

FIG. 2 (color online). Spatial distribution of the longitudinal electric field at the time of maximum absorption $t = t_{\max}$ when the radiation power is maximal for (a) a proton plasma, (b) a deuteron plasma, (c) a plasma of immobile ions. Here, the laser has a trapezoidal temporal profile. The field is normalized by the Compton field $eE_C = m_e c\omega_L$.

The ion mass effect on the angular distribution of photon emission confirms the scenario described above. Each picture shown in Fig. 3 is taken at the time of maximum photon emission $t_{\max}$. In the latter case, the emission in the direction opposite to the laser propagation dominates. It is due to the electrons accelerated in the longitudinal field and escaping from the plasma toward the laser. This is evident from Fig. 3(d), where the electron distribution function is shifted to the negative velocities in the parallel direction and it is symmetric in the perpendicular plane. The electron distribution functions in the case of light ions shown in Figs. 3(c) and 3(d) are significantly different. They are shifted in the forward direction and in the perpendicular plane. Such a distribution function corresponds to the electrons moving as an helix along with the laser pulse. This can be also seen in the angular distribution of the radiation: the maximum of emission is in the forward direction in the case of the protons, while in the deuteron plasma there is still a significant emission in the backward direction. For the case of a proton plasma, about 84% of electrons contributing to the radiation are moving in the direction of laser propagation, whereas, for the case of immobile ions, about 60% of the emitting electrons propagate in the opposite direction.

The electron and photon energy spectra are shown in Fig. 4 for the time near the maximum of radiation emission ($t_{\max} = 22T_L$ for the protons plasma and $40T_L$ for immobile ions). These results are obtained for a Gaussian laser temporal profile. The laser trapezoidal temporal profile gives essentially the same result. The ion mass does not affect the shape of the photon energy spectrum, but, as the spectrum presents the total contribution of all radiating electrons, it just reduces the total photon number and downshifts the position of the maximum to the smaller energy. The position of the maximum $\hbar\omega_{\rm cr}/m_e c^2 \simeq 30$ can

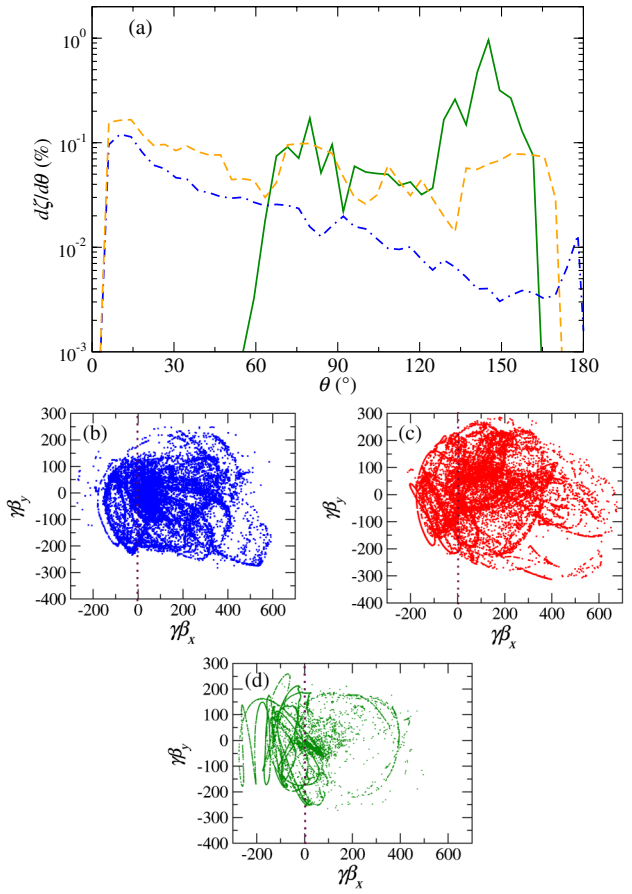

FIG. 3 (color online). (a) Angular distribution of the photon emission with respect to the laser propagation direction (x axis) at the time of maximum emission. (b)–(d) Snapshots of the electron distribution function. Only the electrons with energies exceeding 5 MeV are presented. Color code: (b) blue dots, proton plasma; (c) orange dots, deuteron plasma; (d) green dots, plasma of immobile ions. Here, the laser has a trapezoidal temporal profile.

be readily estimated by knowing $\gamma_e \sim p_e/m_e c \sim a_0 \simeq 200$ and $\mathbf{F}_{Le} \sim m_e c \omega_L a_0 \sqrt{2}$.

In contrast, the modifications of the electron spectrum are rather noticeable. The most significant difference

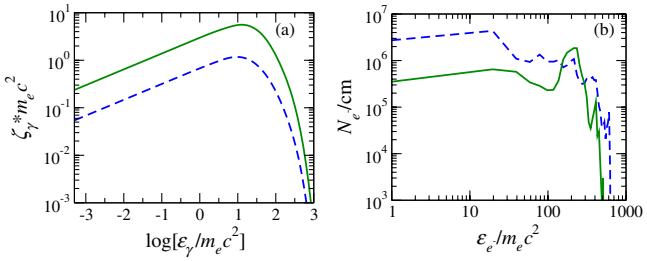

FIG. 4 (color online). Energy distribution of (a) the photon emission and (b) the electron energy distribution at the time of maximum absorption $t = t_{\max}$. Color code: dashed blue lines, proton plasma; solid green lines, plasma of immobile ions. Here, the laser has a Gaussian temporal profile.

resides in the peak of the electron spectrum at $\gamma_e \simeq a_0 \simeq 200$ for the case of immobile ions. These are the electrons that have escaped from the plasma and are moving toward the laser. In the case of the proton plasma, the average electron energy is lower, but a small fraction of electrons is accelerated to energies higher than the quiver energy in the laser field. This is due to the electron stochastic acceleration in the front of the laser pulse [13]. There, the electrostatic field and the laser ponderomotive force are acting in opposite directions, thus permitting the electrons to return several times in the acceleration zone and to gain a higher energy.

The laser-energy absorption dependence on the ion mass is a rather general effect. Our particular choice of parameters $n_e/n_c = 10$ and $a_0 = 200$ illustrates it in detail, but it was also observed for other interaction conditions. Figures 5 and 6 show the dependence of the absorbed laser-energy repartition between the photons η_γ, electrons η_e, and protons η_i on the laser amplitude and the plasma density. The total absorption $\eta_{\text{tot}} = \eta_\gamma + \eta_e + \eta_i$ depends on the ion mass rather weakly. A noticeable difference can be seen in Fig. 5(d) only for extremely high laser intensities corresponding to $a_0 \gtrsim 300$. However, at these intensities, the quantum effects are not negligible anymore. This is demonstrated in Figs. 5(a) and 5(d), where the simulations without the quantum correction $q(\chi_e)$ are shown with the dotted blue and green lines. The quantum effects lead to the saturation of the radiation efficiency at the level of 90% for the laser amplitudes $a_0 \gtrsim 200$ for the case of immobile ions. In contrast, for the case of light ions, the

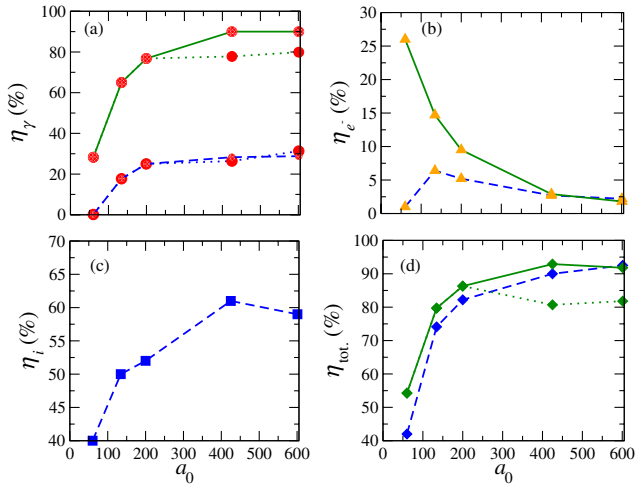

FIG. 5 (color online). Dependence of the laser-energy conversion into photons η_γ (a), into electrons η_e (b), into ions η_i and the total conversion η_{tot} (d) on the laser amplitude a_0 for the plasma density $n_e = 10 n_c$. Color code: dashed blue lines, proton plasma; solid green lines, plasma with immobile ions. The red circles, yellow triangles, and blue squares denote the photons, electrons, and ions, respectively. Here, the laser has a Gaussian temporal profile. The dotted blue and green curves show the simulations without the quantum correction.

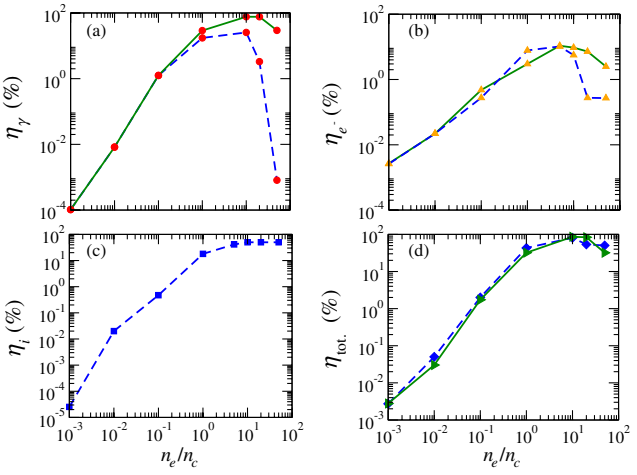

FIG. 6 (color online). Dependence of the laser-energy conversion into photons η_γ (a), into electrons η_e (b), into ions η_i and the total conversion η_{tot} (d) on the plasma density n_e for the laser amplitude $a_0 = 200$. Color code: dashed blue lines, proton plasma; solid green lines, plasma with immobile ions. The red circles, yellow triangles, and blue squares denote the photons, electrons, and ions, respectively. Here, the laser has a Gaussian temporal profile.

quantum correction has a rather small effect on the photon emission, even for the incident laser amplitudes $a_0 = 425$ and 600. This is explained by the fact that the electrons are moving preferentially in the direction of the laser pulse and therefore their quantum parameter χ_e (6) is much smaller in the plasmas with light ions.

The high energy photon emission starts to contribute significantly to the laser-energy absorption for the laser amplitudes $a_0 \gtrsim 80$ in the proton plasma and for even smaller laser amplitudes for the case of heavy ions. For lower laser intensities, the radiation emission does not contribute much to the energy balance, while the laser plasma interaction could still be an efficient source of high energy photons.

It is also interesting to discuss the energy repartition between the electrons and ions. The comparison with the case of immobile ions is not pertinent in this case. This explains a significant difference in the electron absorption at low intensities in Fig. 5(b). The important observation is that the absorbed laser energy is effectively stored in protons and much less in electrons for the laser intensities $a_0 \gtrsim 60$ considered in this Letter. It is expected that more than 50% of the incident laser energy can be transferred to ions for the laser amplitudes $a_0 \gtrsim 100$. This fact agrees with the results of previous publications [3,5,6,14], and it could be rather interesting for fast ion applications in fusion science and medicine [15].

The dependence of the laser-energy absorption on the plasma density in Fig. 6 shows that the density range n_e/n_c between 1 and 20 marks the change of regimes in the case of $a_0 = 200$. For the lower densities, the plasma is transparent for the laser radiation, and the absorption rate increases with the density. In a very underdense plasma, the amplitude of the charge separation field is small, the ions have no influence on the emitted radiation, and the electrons are taking most of the energy from the laser. In contrast, for a proton plasma with a density higher than $20n_c$, the laser piston is formed, and the radiation emission drops down because the electrons are spatially well separated from the laser field [3,6]. The ion acceleration is most efficient in that case. The transition between these two regimes, the induced transparency and the piston, takes place for the electron densities $n_e/n_c \simeq 10$–20. This is comparable with the density of solid hydrogen (100 mg/cc), which corresponds to $n_e/n_c \simeq 50$ for a laser wavelength of 1 μm.

For the laser amplitude $a_0 = 200$ in Fig. 6, the total absorbed laser energy does not significatively depend on the ion mass, even when the quantum effects are negligible. The ion mass mainly affects the laser-energy repartition between photons, electrons, and ions, privileging the electron absorption in the low density plasma and the ion and photon absorption at higher densities.

In conclusion, we have demonstrated that the ion mass strongly affects the radiation generated by accelerated electrons in a high intensity laser plasma interaction. This effect takes place in a limited interval of plasma densities. This is a collective effect that appears due to a stochastic electron motion in the combined laser field and the electrostatic field of charge separation. The ion mass contributes to the spectral composition of the radiation, its angular distribution, and its duration. In the case of light ions (protons or deuterons), the energy of photons is about 10–20 MeV; the pulse duration is 20–30 laser periods, shorter then the laser pulse duration; and the photons are emitted preferentially in the laser propagation direction. The classical electrodynamics is appropriate for describing laser plasma interaction at the dimensionless laser amplitudes as high as 200–300. The electron quantum parameter is not increasing too much with the laser amplitude because the fast electron population is trapped and dragged forward with the laser pulse. It is important to keep the realistic ion-to-electron mass ratio in the numerical simulations in order to describe quantitatively the plasma dynamics and the radiation effects in the strongly relativistic laser fields. The theoretical findings of this Letter can be tested in experiments with solid hydrogen and deuterium targets.

We thank Professor Yasuhiko Sentoku for usage of the code PICLS. Support from the Aquitaine Regional Council and the ANR is also acknowledged.

*capdessus@celia.u-bordeaux1.fr

[1] http://www.extreme-light-infrastructure.eu/.
[2] S. V. Bulanov, Plasma Phys. Control. Fusion **48**, B29 (2006); A. Di Piazza, C. Müller, K. Z. Hatsagortsyan, and C. H. Keitel, Rev. Mod. Phys. **84**, 1177 (2012).

[3] N. Naumova, T. Schlegel, V. T. Tikhonchuk, C. Labaune, I. V. Sokolov, and G. Mourou, Phys. Rev. Lett. **102**, 025002 (2009).
[4] A. Di Piazza, K. Z. Hatsagortsyan, and C. H. Keitel, Phys. Rev. Lett. **102**, 254802 (2009).
[5] M. Tamburini, F. Pegoraro, A. Di Piazza, Ch. H. Keitel, and A. Macchi, New J. Phys. **12**, 123005 (2010).
[6] R. Capdessus, E. d'Humières, and V. T. Tikhonchuk, Phys. Rev. E **86**, 036401 (2012).
[7] http://cilexsaclay.fr.
[8] Y. Sentoku and A. Kemp, J. Comput. Phys. **227**, 6846 (2008).
[9] I. V. Sokolov, J. Exp. Theor. Phys. **109**, 207 (2009).
[10] L. Landau and E. Lifschitz, *The Classical Theory of Fields* (Pergamon, New York, 1994), 4th ed., Vol. 2.
[11] I. V. Sokolov, N. M. Naumova, and J. A. Nees, Phys. Plasmas **18**, 093109 (2011).
[12] C. P. Ridgers, C. S. Brady, R. Duclous, J. G. Kirk, K. Bennett, T. D. Arber, A. P. L. Robinson, and A. R. Bell, Phys. Rev. Lett. **108**, 165006 (2012).
[13] Z. M. Sheng, K. Mima, Y. Sentoku, M. S. Jovanovic, T. Taguchi, J. Zhang, and J. Meyer-ter-Vehn, Phys. Rev. Lett. **88**, 055004 (2002); A. Bourdier, D. Patin, and E. Lefebvre, Physica (Amsterdam) **206D**, 1 (2005).
[14] M. Chen, A. Pukhov, T.-P. Yu, and Z.-M. Sheng, Plasma Phys. Control. Fusion **53**, 014004 (2011).
[15] J. Fuchs, P. Antici, E. d'Humières, E. Lefebvre, M. Borghesi, E. Brambrink, C. A. Cecchetti, M. Kaluza, V. Malka, M. Manclossi, S. Meyroneinc, P. Mora, J. Schreiber, T. Toncian, H. Pépin, and P. Audebert, Nat. Phys. **2**, 48 (2006); L. Robson, P. T. Simpson, R. J. Clarke, K. W. D. Ledingham, F. Lindau, O. Lundh, T. McCanny, P. Mora, D. Neely, C.-G. Wahlstrm, M. Zepf, and P. McKenna, Nat. Phys. **3**, 58 (2007).